



Learning an inverse thermodynamic model for Pneumatic Artificial Muscles control

G. Wang^a, R. Chalard^b, J.A. Cifuentes^c, M.T. Pham^a

^a INSA Lyon, Université Claude Bernard Lyon 1, Ecole Centrale de Lyon, CNRS, Ampère, UMR5005, 69621, Villeurbanne, France

^b Laboratory IBISC, Evry University, Paris-Saclay, 91020 Evry Cedex, France

^c Institute for Research in Technology (IIT), ICAI School of Engineering, Comillas Pontifical University, Calle de Santa Cruz de Marcenado, 26, Madrid, 28015, Spain

ARTICLE INFO

Keywords:

Neural networks

Hybrid modeling

Pneumatic Artificial Muscles

Model-based control

ABSTRACT

Pneumatic Artificial Muscles (PAMs) are highly nonlinear actuators widely used in robotics, rehabilitation, and other dynamic applications. Their complex behavior poses significant challenges for traditional system identification methods. Although machine learning techniques have shown remarkable success in modeling nonlinear systems, their black-box nature often leads to interpretability issues and susceptibility to overfitting. This study proposes a novel hybrid modeling approach that combines the strengths of analytical models with neural networks to capture the inverse thermodynamic behavior of PAMs. The results demonstrate that the hybrid model outperformed both analytical and purely neural network models. The obtained models were further used for model-based control design and the results show that the application of hybrid model improved the tracking performance.

1. Introduction

McKibben Pneumatic Artificial Muscle (PAM) is a biomimetic actuator designed to replicate the behavior of skeletal muscles. Constructed with a flexible rubber inner tube encased in a braided mesh shell, PAMs are sealed at both ends, featuring a gas input on one side and a connection point on the other. Compared to conventional actuators, such as electric and hydraulic actuators, PAMs offer significantly higher power-to-weight and power-to-volume ratios. Due to these characteristics and their similarity to human muscles, PAMs are ideal for the development of rehabilitation therapeutic devices. Successful implementations of PAMs in mechatronic systems for rehabilitation have been previously documented [1–3]. Beyond rehabilitation, PAMs are also utilized in diverse applications, such as bio-robotics, industrial, and aerospace [4,5].

Since the invention of PAM by Gaylord in 1958 [6] and their inception in the 1960s [7] for prosthetic applications, many analytical models of PAMs have been developed for model-based control of higher precision. These models are broadly classified into static and thermodynamic categories. The static models are usually obtained from analyzing the virtual work done by the pressure inside the air chamber and the virtual work done by the external force [8,9]. Additionally,

some studies have employed polynomial equations to capture the relationship between axial tension (F), muscle inner pressure (P), and muscle contraction (ϵ), providing alternative approaches to describe PAM behavior [10,11].

Thermodynamic models, on the other hand, focus on the relationship between the gas mass flow rate (\dot{m}) and the rate of change of internal pressure (\dot{P}) in PAMs. These models are typically used in conjunction with the aforementioned static models to achieve control objectives such as position regulation, trajectory tracking, and force generation. Various approaches have been proposed to model the thermodynamic behavior of PAMs, with the primary distinction lying in the representation of the gas chamber volume (V). Inspired by the work of Chou and Hannaford in [8], some studies have proposed a similar geometry-based framework for the representation of V [12–14]. Alternatively, other studies, including [10,11,15,16] use polynomial approximations of varying degrees to model the volume. Despite these advancements, the accuracy of thermodynamic models remains limited by factors such as gas compressibility and the non-linear elasticity of the bladder, leaving room for further improvement.

In recent decades, Neural Networks (NNs) have demonstrated outstanding performance in modeling nonlinear systems [17,18]. Leveraging this capability, several studies have employed NNs to enhance the

* Corresponding author.

E-mail addresses: genmeng.wang@insa-lyon.fr (G. Wang), remi.chalard@univ-evry.fr (R. Chalard), jacifuentes@comillas.edu (J.A. Cifuentes), minh-tu.pham@insa-lyon.fr (M.T. Pham).

<https://doi.org/10.1016/j.mechatronics.2025.103359>

Received 30 December 2024; Received in revised form 3 April 2025; Accepted 27 May 2025

Available online 19 June 2025

0957-4158/© 2025 The Authors. Published by Elsevier Ltd. This is an open access article under the CC BY license (<http://creativecommons.org/licenses/by/4.0/>).

modeling of PAMs. For instance, [13,19] have developed a Nonlinear Autoregressive with Exogenous Inputs (NARX) model of PAM for real-time control application. Similarly, [10] explored Elman recurrent neural network (RNN) to identify unmodeled dynamics and disturbances in PAM-based actuators. Furthermore, [20] conducted a comparative analysis by integrating a simplified PAM model with various RNN architectures, including Echo State Networks (ESN), Long Short-Term Memory networks (LSTM), and Gated Recurrent Units (GRU). However, RNNs present notable drawbacks: they require large amounts of training data to effectively capture complex temporal patterns and are computationally demanding, often leading to challenges such as vanishing gradients and overfitting, especially when data diversity is limited.

The studies reviewed above indicate that RNN architectures are favored for data-driven modeling of PAMs while thermodynamic modeling of PAMs is often simplified or entirely omitted for model-based control. Therefore a novel physics-informed hybrid approach is proposed to model the thermodynamics of PAMs. This approach integrates an analytical model with a Feedforward Neural Network (FNN), providing a computationally efficient alternative to RNNs while maintaining the adaptability of data-driven methods. Moreover, the hybrid approach enhances model interpretability by incorporating physical insights—shifting from a conventional ‘black-box’ framework, where such insights primarily help define the model’s limitations, to a more transparent ‘gray-box’ paradigm, in which physical knowledge actively guides the training process. By combining the strengths of analytical and data-driven modeling, this method is expected to achieve improved accuracy, generalization, and efficiency. To validate its effectiveness, the hybrid model will be compared against LSTM networks, FNNs with equivalent number of parameters, and a standalone analytical model. Capabilities such as generalization to unseen dynamics, and robustness to limited training data will be assessed.

Numerous studies have explored the integration of RNN models into real-time control loops for the regulation of PAMs. For instance, Elman networks have been employed to enhance the accuracy of analytical models, thereby improving the performance of model-based control strategies [10]. Similarly, ESNs have been utilized to predict the future dynamics of a PAM-driven exoskeleton, enabling the implementation of nonlinear model predictive control (NMPC) [21]. Beyond the application of RNNs to PAM control, many studies have explored the use of different neural network models for PAM control, demonstrating promising results [22–24]. In this context, the model proposed in the present study is also considered for its potential applicability in PAM control once trained. To this end, the control performance of the learned inverse thermodynamic model in position control is evaluated and compared against both analytical models and other learned approaches.

The structure of this document is organized as follows: Section 2 details the adapted analytical model and the proposed physics-informed hybrid approach. Section 3 provides a comprehensive description of the datasets preparation and experimental setup. Section 4 presents a comparative analysis of the hybrid model’s performance against other baseline models, as well as its application to a position control problem. Finally, Section 5 concludes by summarizing the key findings and discussing potential directions for future research.

2. Design of the hybrid model

2.1. Analytical model

Based on the first law of thermodynamics, the change of internal energy \dot{U} of PAM is described by:

$$\dot{U} = Q_{in} - Q_{out} + kC_v(\dot{m}_{in}T_{in} - \dot{m}_{out}T) - \dot{W} \quad (1)$$

where Q_{in} and Q_{out} are the heat transfer terms, \dot{m}_{in} and \dot{m}_{out} are the mass flows entering and leaving the chamber, k is the specific heat ratio, C_v

denotes the specific heat at constant volume, T_{in} is the temperature of the incoming air flow, T is the temperature inside the chamber, \dot{W} is the rate of change in work done by the inner pressure. To facilitate the modeling process, several simplifying assumptions are employed: (i) the gas is considered to behave as an ideal gas, (ii) the pressure and temperature are assumed to be uniformly distributed within each chamber, and (iii) kinetic and potential energy contributions are deemed negligible. Under these conditions, the time derivative of the internal pressure \dot{P} within the PAM is defined as:

$$\dot{P} = \frac{kRT}{V}(\dot{m}_{in} - \dot{m}_{out}) - k\frac{\dot{V}}{V}P + (k-1)\frac{P}{V}(Q_{in} - Q_{out}) \quad (2)$$

R is the ideal gas constant, V the volume of PAM and \dot{V} the change rate of V . Furthermore, if the process is considered to be adiabatic ($Q_{in} - Q_{out} = 0$), the equation simplifies to:

$$\dot{P} = \frac{kRT}{V}(\dot{m}_{in} - \dot{m}_{out}) - k\frac{\dot{V}}{V}P \quad (3)$$

This simplified thermodynamic model, first introduced by [25], has been widely adopted in the research related to PAMs. For example, [15] extended this model by incorporating a specific representation of the PAM volume, expressed as:

$$V = D_1\varepsilon^2 + D_2\varepsilon + D_3 \quad (4)$$

where D_1 , D_2 and D_3 are the parameters to be identified. This proposed model of PAM volume is based on its deformation using a low-order polynomial, where the parameters lack physical meaning, making it difficult to derive insights into the underlying process being modeled. However, this model provides a good balance between simplicity and precision for the intended application. A more refined polynomial approximation of the volume could be considered, but this would come at the cost of identifying additional D_i coefficients. Later, [26] also adopted (3) in their model-based control approach, but proposed a different calculation of V based on its geometrical characteristics such as the initial braid angle α_0 , the initial diameter of the cylinder D_0 , the initial length of the muscle l_0 as well as non-extensibility of threads in the braided mesh shell.

$$V = \frac{\pi D_0^2 l_0}{4} \left[\frac{1}{\sin^2 \alpha_0} - \frac{(1-\varepsilon)^\gamma}{\tan^2 \alpha_0} \right] (1-\varepsilon) \quad (5)$$

The volume can be well approximated with the carefully chosen parameter γ . Then by assuming the volume change due to pressure variations $\frac{\partial V}{\partial P}$ is negligible, the derivative of volume \dot{V} can be expressed as in [14]:

$$\dot{V} = \frac{\partial V}{\partial \varepsilon} \dot{\varepsilon} = \frac{\pi D_0^2 l_0}{4} \left[-\frac{1}{\sin^2 \alpha_0} + (\gamma+1)\frac{(1-\varepsilon)^\gamma}{\tan^2 \alpha_0} \right] \dot{\varepsilon} \quad (6)$$

By introducing (5)–(6) into (3), a detailed thermodynamic model of PAM can be obtained. However, when it comes to model-based control design, the servo valve to be controlled often requires a desired mass flow $\dot{m} = \dot{m}_{in} - \dot{m}_{out}$. Therefore (3) is usually used inversely to determine desired mass flow \dot{m} given a desired system dynamic as in [11,26,27]. This inverse formulation is described by:

$$\dot{m} = \frac{\dot{P}V}{kRT} + \frac{PV}{RT} \quad (7)$$

By selecting appropriate parameters, such as the specific heat ratio for air $k = 1.4$, the gas constant for dry air $R = 287 \text{ J}/(\text{kg} \cdot \text{K})$, and the temperature $T = 293 \text{ K}$, inverse model (7) becomes the analytical foundation for constructing the proposed hybrid model in this study.

2.2. Hybrid model

In this study, the term ‘hybrid’ refers to the integration of an NN model with an analytical model. Several hybridizing strategies have been proposed in the literature, each leveraging the strengths of both methodologies. For example, [10] trained an NN model to compensate

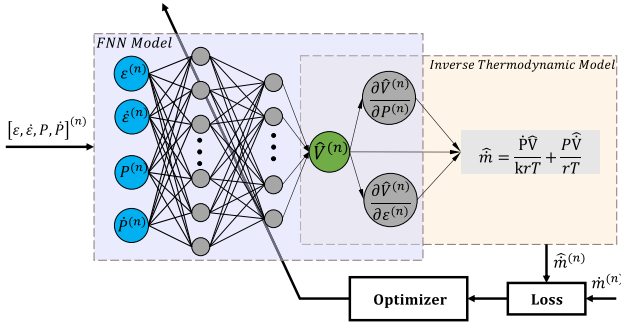


Fig. 1. Proposed hybrid model for inverse thermodynamic of PAM.

for the discrepancies between the outputs of an analytical model and the experimental measurements, thus enhancing the model. Another notable example is the work of [28], who introduced Physics-Informed Neural Networks (PINNs). PINNs utilize an analytical model to guide the NN training in a supervised manner by encoding the physical principles of the system into the loss function. Similarly, [29] proposed the Deep Lagrangian Network (DeLaN), which incorporates Lagrangian mechanics into the network structure to estimate the inertial matrix of robotic systems in an unsupervised manner. Both PINNs and DeLaN are made possible by advances in modern automatic differentiation techniques, allowing the seamless integration of differential equations into the NN architecture. This enables the encoding of prior physical knowledge directly into the network topology.

The hybrid model (HM) proposed in this study integrates a two-hidden-layer FNN with an inverse thermodynamic model (7) of PAMs, as depicted in Fig. 1. The role of FNN model is to estimate the volume of PAM based on the network inputs:

$$\hat{V} = \hat{V}(\varepsilon, \dot{\varepsilon}, P, \dot{P}; \theta) \quad (8)$$

where θ is NN model parameters. By leveraging automatic differentiation tools, the derivative of V of PAM w.r.t contraction ε and inner pressure P , i.e. $\frac{\partial \hat{V}^{(n)}}{\partial \varepsilon^{(n)}}$ and $\frac{\partial \hat{V}^{(n)}}{\partial P^{(n)}}$ can be obtained in parallel to $\hat{V}^{(n)}$. Next, \hat{V} can be calculated as follows:

$$\hat{V} = \frac{\partial \hat{V}}{\partial \varepsilon} \dot{\varepsilon} + \frac{\partial \hat{V}}{\partial P} \dot{P} \quad (9)$$

The thermodynamic model, integrated into the hybrid framework, uses the computed volume \hat{V} and its derivatives to estimate the mass flow $\hat{m}^{(n)}$ who has caused the system to behave as described in inputs $[\varepsilon, \dot{\varepsilon}, P, \dot{P}]^{(n)}$ at the same time step t^n . The prediction error can be measured with trusted mass flow value $\dot{m}^{(n)}$ in mean squared error (MSE) loss function as in (10). Then by minimizing the loss between predictions and target values, we can find NN parameters θ^* that satisfies a desired performance of hybrid model. The process of optimization is described by

$$\theta^* = \underset{\theta}{\operatorname{argmin}} \left(\frac{1}{N} \sum_{n=1}^N (\hat{m}_{HM}^{(n)} - \dot{m}^{(n)})^2 + \frac{\lambda}{2} \|\theta\|_2^2 \right) \quad (10)$$

where θ^* represents the NN parameters, λ is the weight decay and the learned HM \hat{f}_{HM} is then described by :

$$\hat{m}_{HM} = \hat{f}_{HM}(\varepsilon, \dot{\varepsilon}, P, \dot{P}; \theta^*) \quad (11)$$

where

$$\hat{f}_{HM}(\varepsilon, \dot{\varepsilon}, P, \dot{P}; \theta) = \left(\frac{P}{rT} \frac{\partial \hat{V}}{\partial P} + \frac{\hat{V}}{krT} \right) \dot{P} + \frac{P}{rT} \frac{\partial \hat{V}}{\partial \varepsilon} \dot{\varepsilon} \quad (12)$$

2.3. Baselines

To evaluate the predictive performance of the hybrid model \hat{f}_{HM} , its mass flow prediction is compared against three baseline models: an

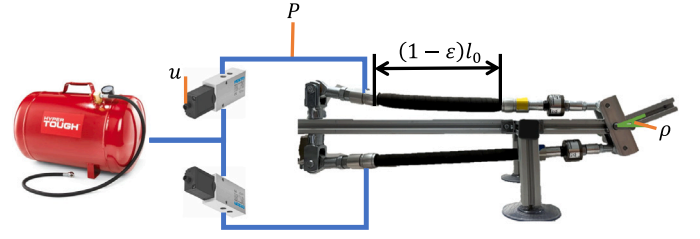


Fig. 2. Test bench for data collection.

analytical inverse thermodynamic model \hat{f}_{AM} , a FNN model \hat{f}_{FNN} and a LSTM model \hat{f}_{LSTM} .

For the analytical model (AM) the mass flow is computed using (5)–(7), as the parameters have been previously identified for the same type of PAMs under similar operating conditions. The mass flow prediction from the AM is expressed as:

$$\hat{m}_{AM} = \hat{f}_{AM}(\varepsilon, \dot{\varepsilon}, P, \dot{P}; \gamma) \quad (13)$$

Concurrently, a FNN network and a LSTM network were implemented to learn from the same training data used for \hat{f}_{HM} . The process of fitting these two models can be described by:

$$\phi^* = \underset{\phi}{\operatorname{argmin}} \frac{1}{N} \sum_{n=1}^N (\hat{m}_{FNN}^{(n)} - \dot{m}^{(n)})^2 \quad (14)$$

$$\psi^* = \underset{\psi}{\operatorname{argmin}} \frac{1}{N} \sum_{n=1}^N (\hat{m}_{LSTM}^{(n)} - \dot{m}^{(n)})^2 \quad (15)$$

where ϕ and ψ are model parameters. Unlike the hybrid model, the FNN and LSTM models are purely data-driven and do not incorporate any analytical model into their structure. Therefore, the mass flow predictions for these two models are directly derived from the input variables $[\varepsilon, \dot{\varepsilon}, P, \dot{P}]$, as described by:

$$\hat{m}_{FNN} = \hat{f}_{FNN}(\varepsilon, \dot{\varepsilon}, P, \dot{P}; \phi^*) \quad (16)$$

$$\hat{m}_{LSTM} = \hat{f}_{LSTM}(\varepsilon, \dot{\varepsilon}, P, \dot{P}; \psi^*) \quad (17)$$

3. Experiments

3.1. Training dataset preparation

Data were collected using the test bench shown in Fig. 2, a prototype designed for ankle rehabilitation training. A pair of antagonistically linked PAMs were used to simulate the muscles of the anterior and posterior calf to actuate this prototype. While both PAMs were activated during the experiments, only data from the upper muscle were used for model training as they were identical and exhibited symmetrical dynamics in the experiments.

The test bench includes an inclinometer and a pressure sensor to measure the ankle angle ρ and internal pressure P . The contraction ratio ε is then calculated from the ankle angle using the prototype's geometric model. A simple proportional derivative (PD) controller is used to make the rotating part of the test bench follow desired trajectories, from which the sensor data can be used directly or indirectly to construct the numerical training dataset $[\varepsilon, \dot{\varepsilon}, P, \dot{P}; \dot{m}]$. The target values \dot{m} that causes the change in internal pressure are derived from the internal pressure P and the input control voltage u with a proportional directional control valve (PDCV) model, as described in [30]. The data collection covered eight distinct trajectories of reference sinusoidal signal in ρ , combining different amplitudes [2, 5, 7.5, 10] degrees and frequencies [0.5, 1] rad/s.

Table 1
The hyperparameters of NN model and hybrid approaches.

	HM, FNN	LSTM
Network dimension	2×128	2×37
Number of parameters	17 320	17 551
Activation function	SoftPlus	Sigmoid + Tanh
Batch size		1024
Learning rate		$1e-4$
Weight decay		$1e-5$
Optimizer		Adam
Loss function	Mean Squared Error (MSE)	
Number of epochs	10 000	
PyTorch initialization seed	66	

Table 2
Prediction error of baselines and hybrid approaches calculated in MSE.

	Baselines			Hybrid model	Unit
	Analytical model	FNN model	LSTM model		
Train	0.1781	0.0090	0.0055	0.1029	
Task 1	0.2112	0.1434	0.4402	0.2027	NL^2/min^2
Task 2	17.4198	40.8870	57.7349	3.1999	
Task 3	3.9158	2.3689	1.6775	0.2905	

3.2. Hybrid model and baseline models training

To minimize the impact of non-model structural differences on performance, the hyperparameters were kept as consistent as possible across all models. Table 1 presents the hyperparameters chosen for the training of the three data-driven models. The hyperparameters of the hybrid model and the FNN model were kept identical to ensure that any performance differences observed between them would be attributed solely to the structural differences, specifically the inclusion of the analytical model in the hybrid approach.

For the LSTM model, despite maintaining the same number of hidden layers, the dimensionality of the hidden layer states was reduced to match the approximate parameter count of the other two models. Additionally, the activation function in the LSTM cell can only be restricted to a selection different from the two previous models. The same optimizer, learning rate, and number of epochs were used for all models, with these hyperparameters being selected based on the experience acquired from extensive training of various models. The obtained model parameters θ^* , ϕ^* , ψ^* will be used for benchmarking against the analytical model during the testing phase.

3.3. Test datasets preparation

The test datasets were designed to evaluate the performance of the hybrid and baseline models under unseen dynamics. The test datasets consist of eighteen trajectories that differ from the training data in terms of frequency, amplitude, and signal type: (1) the first group is obtained by following sinusoidal reference trajectories at a lower frequency, i.e., 0.2 rad/s, with a broader range of amplitudes i.e., $[2, 5, 7.5, 10, 15, 20]$ degrees than the training dataset; (2) The second group has the same amplitudes, same signal type but at a higher frequency, i.e., 4 rad/s; and (3) The third group uses the same amplitude and frequency as the training data, i.e., 1 rad/s, but with triangular signals. These variations introduce new system dynamics, where lower frequencies correspond to smaller gas flows and higher frequencies to larger flows. The triangular signals further challenge the models with different dynamic features.

3.4. Hybrid model and baselines testing

In the testing phase, the model parameters θ^* , ϕ^* , ψ^* obtained from the training phase were used to form \hat{f}_{HM} , \hat{f}_{FNN} and \hat{f}_{LSTM} . These

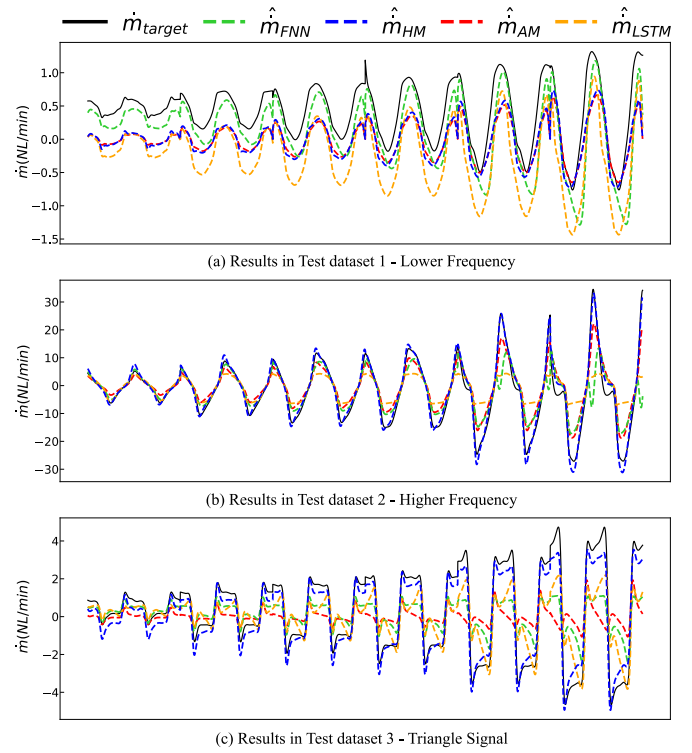


Fig. 3. Prediction Results of different models in different tasks.

were compared with the analytical model, described by (5)–(6), to assess the prediction performance on the test datasets. The predictions of the four models, \hat{m}_{HM} , \hat{m}_{AM} , \hat{m}_{FNN} , and \hat{m}_{LSTM} , were compared with the target value \dot{m} . The results are presented in the following section.

4. Results and discussion

4.1. Results in prediction

The prediction accuracy of the models across different datasets is summarized in Table 2, where the MSE between predicted values \hat{m} and target values \dot{m} is used as the evaluation metric. The best performance for each task is highlighted in bold. It is observed that in Task 1 (lower frequency), the hybrid model performs worse than the FNN model, but closer to the analytical model and better than the LSTM model. As shown in the first row of Fig. 3, the green dashed line (FNN) is closest to the target values (black solid line), followed by the blue dashed line (HM) and the red dashed line (AM), while the lowest fit with the target is the orange dashed line (LSTM). The numerical values in Table 2 confirm this observation from Fig. 3, indicating that the hybrid model (HM) performs slightly better than the analytical model (AM) due to its smaller MSE. In Tasks 2 and 3 (higher frequency and triangular signals), the hybrid model shows clear improvements in prediction accuracy over all other models. The reduced performance of hybrid model in Task 1 may be attributed to the smaller airflow rates at lower dynamic frequencies, which limit the PDCV activation range. In this range, the system becomes more susceptible to external disturbances, such as friction in the valves, and the hybrid approach struggles to accurately predict the target airflow \dot{m} through the volume \hat{V} and its derivatives $\frac{\partial \hat{V}}{\partial \epsilon}$ and $\frac{\partial \hat{V}}{\partial P}$. Additionally, the dynamics that occur at lower frequencies may not have been fully captured by the training dataset, leading to reduced model performance.

In contrast, the FNN and LSTM models perform significantly worse in Tasks 2 and 3. As seen in Fig. 3(b) and (c), the deviations between

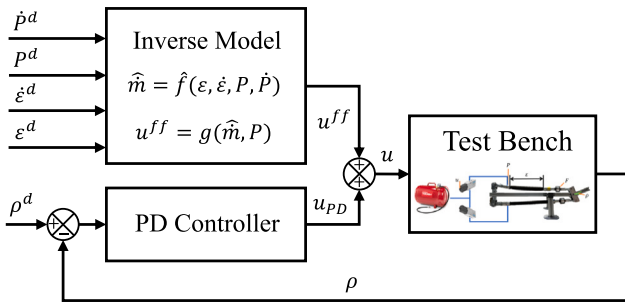


Fig. 4. Real-time control loop.

the predicted and actual values for these models are more pronounced compared to the hybrid model. This suggests that the higher frequency and amplitude in these tasks introduced scenarios that were not well-represented in the training data. The lack of physics-based priors likely impacted the models' ability to generalize, resulting in less stability compared to the hybrid approach. The hybrid model consistently outperforms all other models in tasks requiring generalization to unseen data. As shown in Fig. 3, the hybrid model provides significantly better predictions in dynamic scenarios like Task 2 (higher frequency) and Task 3 (triangular signals).

Generally, the hybrid model demonstrates superior prediction accuracy compared to the analytical model across all datasets. However, the LSTM and FNN model outperforms the hybrid model in the train dataset and the FNN model outperforms the hybrid model in the Task 1.

The LSTM model performs well on the training data but struggles to generalize to unseen scenarios, indicating that it may have learned specific patterns in the training data that do not translate well to new conditions. Meanwhile, among the three tasks prepared for testing, the FNN model achieves only slightly better accuracy than the hybrid model in Task 1 which requires a smaller prediction range than the training dataset. This observation reinforces the superior generalization capability of the hybrid model, which shows a more balanced performance between training and testing. However, the significantly higher error values in the test datasets for Tasks 2 and 3 in the FNN and LSTM models suggest in parallel the presence of overfitting.

All models were trained for 10000 epochs with a learning rate of $1e^{-4}$, a configuration selected to strike an optimal balance between computational efficiency and model accuracy. While further optimization may be possible, the results already indicate that the hybrid model improves upon the analytical model in all datasets and outperforms the baseline models in two out of four tasks. This demonstrates that combining analytical models with neural networks offers a robust and scalable approach for modeling complex nonlinear systems like PAMs. The hybrid approach not only achieves high accuracy but also ensures adaptability, making it suitable for dynamic applications while minimizing computational overhead.

4.2. Results in real-time control

In this section, HM, AM and FNN have been extrapolated and applied to a model-based control design for the manipulator shown in Fig. 2. The control law is described as:

$$u = K_p(\rho_d - \rho) + K_d(\dot{\rho}_d - \dot{\rho}) + u^{ff} \quad (18)$$

with u^{ff} is the precompensation term calculated using different models and K_p , K_d are the controller gains. The inverse PDCV model $g(\hat{m}, P)$ is considered as static and is approximated using polynomial fitting of experimental data from [30]. Given the estimated mass flow \hat{m} and P pressure, the control input u can then be precompensated by u^{ff} .

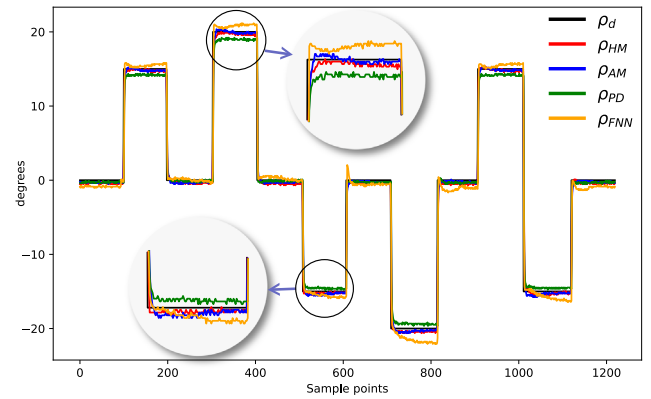
Fig. 5. Desired joint angle ρ_d and actual joint angles ρ by different controller.

Table 3

MSE between ρ_d and ρ .

Controller	PD	AM+PD	FNN+PD	HM+PD
MSE	3.61	2.18	3.55	1.95

The control target is to follow some step signals ρ_d as shown in Fig. 5. The manipulator was firstly controlled using a simple PD controller to get rough inputs $[\epsilon, \dot{\epsilon}, P, \dot{P}]$ for obtained system dynamics \hat{f} , which were then processed to match the desired system dynamics more accurately for tracking ρ_d . The optimized inputs $[\epsilon^d, \dot{\epsilon}^d, P^d, \dot{P}^d]$ are used for precompensation in real-time control, as shown in Fig. 4.

The performance of the control system using the models \hat{f}_{HM} , \hat{f}_{FNN} and \hat{f}_{AM} is compared in Fig. 5. For each control design, the PD controller was optimized individually to achieve the best possible control performance. Additionally, the desired tracking signal includes dynamic behaviors that were not present in the training dataset, providing further insight into how each model handles unseen dynamics in real-time control.

Overall, the model-based control method outperforms the simple PD controller when tracking nonlinear targets like ρ_d . The hybrid and analytical models, when used with the PD controller, achieve smaller position errors compared to the FNN model. Although the performance of the hybrid and analytical models is nearly identical, as shown in Table 3, the hybrid model exhibits slightly better results than the analytical model in real-time control experiments.

5. Conclusion

An increasing number of researchers have embraced the idea of combining physical knowledge with NN to model complex nonlinear systems, particularly since the introduction of PINNs. This study highlights the potential of hybrid models that integrate analytical/physical and NN approaches. As modeling PAMs systems with a system identification approach is an ongoing challenge and the hybrid approaches have shown promising performance, this study bridges the gap of modeling PAMs using a hybrid approach.

The results obtained in this study show that the hybrid model generally outperforms an analytical model, a FNN model given the same network structure and a LSTM model using the same datasets. The experimental results also showed that the proposed hybrid model helps improve position control of a pair of antagonistic muscles. There remains, however, potential for further improvements. Future research could focus on incorporating additional dynamics such as friction and mechanical interactions, as well as expanding the training dataset to improve model performance.

The hybrid model is planned to be applied in future work to complete the development of a force and position control method for a medical simulator prototype.

CRediT authorship contribution statement

G. Wang: Writing – review & editing, Writing – original draft, Software, Project administration, Methodology, Investigation, Data curation, Conceptualization. **R. Chalard:** Writing – review & editing, Supervision, Methodology. **J.A. Cifuentes:** Writing – review & editing, Methodology. **M.T. Pham:** Writing – review & editing, Supervision, Methodology.

Declaration of competing interest

The authors declare that they have no known competing financial interests or personal relationships that could have appeared to influence the work reported in this paper.

Data availability

Data will be made available on request.

References

- [1] Noritsugu T, Tanaka T. Application of rubber artificial muscle manipulator as a rehabilitation robot. 1997;2.
- [2] Ding M, Ueda J, Ogasawara T. Pinpointed muscle force control using a power-assisting device: System configuration and experiment. 2008, p. 186. <http://dx.doi.org/10.1109/BIOROB.2008.4762829>.
- [3] Park Y-L, Santos J, Galloway KG, Goldfield EC, Wood RJ. A soft wearable robotic device for active knee motions using flat pneumatic artificial muscles. In: 2014 IEEE international conference on robotics and automation. ICRA, Hong Kong, China: IEEE; 2014, p. 4805–10. <http://dx.doi.org/10.1109/ICRA.2014.6907562>.
- [4] Wereley N, Kothera C, Bubert E, Woods B, Gentry M, Vocke R. Pneumatic artificial muscles for aerospace applications. In: 50th AIAA/ASME/ASCE/AHS/ASC structures, structural dynamics, and materials conference. Structures, structural dynamics, and materials and co-located conferences, American Institute of Aeronautics and Astronautics; 2009, <http://dx.doi.org/10.2514/6.2009-2140>.
- [5] Andrikopoulos G, Nikolakopoulos G, Manesis S. A survey on applications of pneumatic artificial muscles. In: 2011 19th mediterranean conference on control & automation. MED, Corfu, Greece: IEEE; 2011, p. 1439–46. <http://dx.doi.org/10.1109/MED.2011.5982983>.
- [6] Gaylord RH. Fluid actuated motor system and stroking device. 1958, US Patent US2844126A.
- [7] McKibben JL. Artificial muscle. *Life Mag* 1960;87–8, March 14.
- [8] Chou C-P, Hannaford B. Measurement and modeling of McKibben pneumatic artificial muscles. *IEEE Trans Robot Autom* 1996;12(1):90–102. <http://dx.doi.org/10.1109/70.481753>.
- [9] Tondou B, Lopez P. Modeling and control of McKibben artificial muscle robot actuators. *IEEE Control Syst* 2000;20(2):15–38. <http://dx.doi.org/10.1109/37.833638>.
- [10] Hošovský A, Pitel' J, Židek K. Enhanced dynamic model of pneumatic muscle actuator with elman neural network. *Abstr Appl Anal* 2015;2015:1–16. <http://dx.doi.org/10.1155/2015/906126>.
- [11] Hildebrandt A, Sawodny O, Neumann R, Hartmann A. A cascaded tracking control concept for pneumatic muscle actuators. In: 2003 European control conference. ECC, Cambridge, UK: IEEE; 2003, p. 2517–22. <http://dx.doi.org/10.23919/ECC.2003.7085344>.
- [12] Kopečný L, Zalud L. Measurements for the thermodynamic model of a pneumatic muscle actuator. In: Mason A, Mukhopadhyay SC, Jayasundera KP, editors. Sensing technology: Current status and future trends III. Cham: Springer International Publishing; 2015, p. 359–76. http://dx.doi.org/10.1007/978-3-319-10948-0_18.
- [13] Chavoshian M, Taghizadeh M, Mazare M. Hybrid dynamic neural network and PID control of pneumatic artificial muscle using the PSO algorithm. *Int J Autom Comput* 2020;17(3):428–38. <http://dx.doi.org/10.1007/s11633-019-1196-5>.
- [14] Saba DB, Massioni P, Bideaux E, Brun X. Flatness-based control of a two-degree-of-freedom platform with pneumatic artificial muscles. 2017, <http://dx.doi.org/10.48550/arXiv.1703.05503>, arXiv:1703.05503 [eess].
- [15] Itto T, Kogiso K. Hybrid modeling of McKibben pneumatic artificial muscle systems. In: 2011 IEEE international conference on industrial technology. Auburn, AL, USA: IEEE; 2011, p. 65–70. <http://dx.doi.org/10.1109/ICIT.2011.5754347>.
- [16] Shin T, Ibayashi T, Kogiso K. Detailed dynamic model of antagonistic PAM system and its experimental validation: Sensorless angle and torque control with UKF. *IEEE/ASME Trans Mechatronics* 2022;27(3):1715–26. <http://dx.doi.org/10.1109/TMECH.2021.3086218>.
- [17] Brunton SL, Kutz JN. Data-driven science and engineering: Machine learning, dynamical systems, and control. Cambridge: Cambridge University Press; 2019, <http://dx.doi.org/10.1017/9781108380690>.
- [18] Wang G, Chalard R, Cifuentes JA, Pham MT. Physics-Informed Hybrid Modeling of Pneumatic Artificial Muscles. In: 2025 IEEE International Conference on Robotics and Automation (ICRA). ICRA, Atlanta, United States: IEEE; 2025.
- [19] Ahn KK, Anh HPH. Comparative study of modeling and identification of the pneumatic artificial muscle (PAM) manipulator using recurrent neural networks. *J Mech Sci Technol* 2008;22(7):1287–98. <http://dx.doi.org/10.1007/s12206-008-0416-7>.
- [20] Sun W, Akashi N, Kuniyoshi Y, Nakajima K. Physics-informed recurrent neural networks for soft pneumatic actuators. *IEEE Robot Autom Lett* 2022;7(3):6862–9. <http://dx.doi.org/10.1109/LRA.2022.3178496>.
- [21] Cao Y, Huang J. Neural-network-based nonlinear model predictive tracking control of a pneumatic muscle actuator-driven exoskeleton. *IEEE/CAA J Autom Sin* 2020;7(6):1478–88. <http://dx.doi.org/10.1109/JAS.2020.1003351>.
- [22] Zhang H, Fan J, Qin Y, Tian M, Han J. Active neural network control for a wearable upper limb rehabilitation exoskeleton robot driven by pneumatic artificial muscles. *IEEE Trans Neural Syst Rehabil Eng* 2024;32:2589–97. <http://dx.doi.org/10.1109/TNSRE.2024.3429206>.
- [23] Fan J, Zhong J, Zhao J, Zhu Y. BP neural network tuned PID controller for position tracking of a pneumatic artificial muscle. *Technol Health Care* 2015;23:S231–238. <http://dx.doi.org/10.3233/THC-150958>, arXiv:26410488.
- [24] Liu G, Sun N, Liang D, Chen Y, Yang T, Fang Y. Neural network-based adaptive command filtering control for pneumatic artificial muscle robots with input uncertainties. *Control Eng Pract* 2022;118:104960. <http://dx.doi.org/10.1016/j.conengprac.2021.104960>.
- [25] Richer E, Hurmuzlu Y. A high performance pneumatic force actuator system: Part I—Nonlinear mathematical model. *J Dyn Syst Meas Control* 2000;122(3):416–25. <http://dx.doi.org/10.1115/1.1286336>.
- [26] Bou Saba D, Bideaux E, Brun X, Massioni P. A complete model of a two degree of freedom platform actuated by three pneumatic muscles elaborated for control synthesis. In: BATH/ASME 2016 symposium on fluid power and motion control. ASME proceedings, vol. V001T01A004, 2016, <http://dx.doi.org/10.1115/FPMC2016-1706>.
- [27] Chikh L, Poignet P, Pierrot F, Michelin M. A generalized predictive force controller for electropneumatic cylinders. *IFAC Proc Vol* 2010;43(14):1058–63.
- [28] Raissi M, Perdikaris P, Karniadakis GE. Physics informed deep learning (part I): Data-driven solutions of nonlinear partial differential equations. 2017.
- [29] Lutter M, Ritter C, Peters J. Deep lagrangian networks: Using physics as model prior for deep learning. 2019, <http://dx.doi.org/10.48550/arXiv.1907.04490>, arXiv:1907.04490 [cs, eess, stat].
- [30] Olaby O, Brun X, Sesmat S, Redarce T, Bideaux E. Characterization and modeling of a proportional valve for control synthesis. In: 6th JFPS international symposium on fluid power. Tsukuba, Japan; 2005, <http://dx.doi.org/10.5739/isfp.2005.771>.